

Mathematical Modeling of the Biomechanics of the Lamina Cribrosa Under Elevated Intraocular Pressures

Tim Newson¹

Associate Professor
Geotechnical Research Centre,
Department of Civil and Environmental
Engineering,
University of Western Ontario,
London, Ontario, N6A 5B9, Canada
e-mail: tnewson@eng.uwo.ca

Ahmed El-Sheikh

Senior Lecturer
Division of Civil Engineering,
University of Dundee,
Dundee DD1 4HN Scotland, United Kingdom
e-mail: a.i.h.elsheikh@dundee.ac.uk

Comprehensive understanding of the biomechanical performance of the lamina cribrosa (LC) and the optic nerve head is central to understanding the role of elevated intraocular pressures (IOP) in chronic open angle glaucoma. In this paper, six closed-form mathematical models based on different idealizations of the LC are developed and compared. This approach is used to create further understanding of the biomechanical behavior by identifying the LC features and properties that have a significant effect on its performance under elevated IOP. The models developed are based on thin circular plate and membrane theories, and consider influences such as in-plane pretension caused by scleral expansion and large deflections. Comparing the results of the six models against a full ocular globe finite element model suggests the significance of the in-plane pretension and the importance of assuming that the sclera provides the LC with a clamped edge. The model that provided the most accurate representation of the finite element model was also used to predict the behavior of a number of LC experimental tests presented in the literature. In addition to the deflections under elevated IOP, the model predictions include the distributions of stress and strain, which are shown to be compatible with the progression of visual field loss experienced in glaucoma.

[DOI: 10.1115/1.2205372]

Keywords: lamina cribrosa, mathematical modeling, glaucoma, plate analysis, membrane analysis

1 Introduction

Glaucoma is a major cause of irreversible blindness in Europe and North America and the third most common cause of blindness worldwide. Chronic open angle glaucoma affects 1% of the population over 40 and more than 10% over 80. The hypothesis of pressure-dependent glaucomatous optic neuropathy, in which the elevation of intraocular pressure (IOP) causes optic nerve damage and hence visual impairment, is generally accepted. Reference can be made for example to Anderson [1], Emery et al. [2], Quigley [3], and Harju [4]. In this hypothesis, the primary site of damage is the lamina cribrosa (see Fig. 1), which is the main supporting component of the optic nerve head. The lamina cribrosa (LC) is a very thin structure located in the center of the optic nerve head, through which the optic nerve fibers (axons) pass. Retrodisplacement of the LC under elevated IOP is thought to cause structural damage to the axons and reduce blood flow, leading to loss of vision as reported by Levy and Crapps [5] and Quigley et al. [6]. This relationship between the LC deformation and the axonal damage is not yet fully understood, although the association between the two phenomena is thought to be significant.

Several efforts have been made to date to link LC deformation and the resulting stresses and strains to axonal damage. Mathematical techniques idealizing the LC as a homogenous structure and employing either plate or membrane analogy have been used because of the apparently simple geometry of the LC. These efforts include an attempt by Chi et al. [7] to idealize the LC as a membrane (i.e., assuming no flexural resistance) with a resulting overestimation of deformation under IOP. Dongqi and Zeqin [8]

later developed a mathematical model for a thin elastic circular plate representing an idealized LC. The model considered the effect of both the IOP and the in-plane pretension due to scleral expansion, although the in-plane pretension was not directly related to the value of the IOP. This was followed by another effort by Edwards and Good [9]. Their model was different in two ways: it ignored the in-plane pretension caused by scleral expansion and was based on a large deflection idealization of the LC. The model was extended to predict the stresses and strains experienced by the optic nerve axons due to IOP, hence, providing a further step by attempting to relate IOP elevation to axonal injury.

These models and other contributions (such as Bellezza [10]) have led to notable advances in our understanding of the LC biomechanics and the complexity of its structure. The degree of fixity offered by the connection with the sclera, the influence of the pretension caused by scleral expansion and the ratio between flexural and in-plane stiffness are among the factors that could have a strong effect on the structure and accuracy of the mathematical model representing the LC behavior.

Instead of adopting one set of assumptions (regarding the importance of these factors) in developing a mathematical model, this research follows a different strategy. It considers six modeling techniques built on different combinations of modeling idealizations, which consider how the aforementioned factors should be incorporated into the models. By assessing and comparing these techniques the importance of each factor is determined.

This approach should be seen as a first step towards the development of more complex and potentially more accurate models, and also provides relatively simple and usable mathematical models for preliminary assessment of problems. Similar research to assess the effect of other issues such as anisotropy and viscoelas-

¹Corresponding author.

Contributed by the Bioengineering Division of ASME for publication in the JOURNAL OF BIOMECHANICAL ENGINEERING. Manuscript received December 13, 2004; final manuscript received February 3, 2006. Review conducted by Michael Sacks.

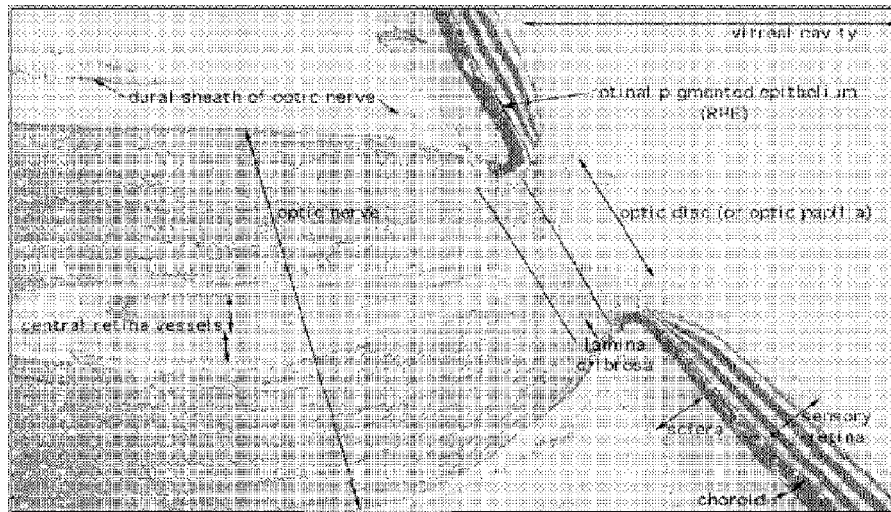


Fig. 1 Cross section through the human optic nerve head

tivity is currently underway. The results of this work could also help improve understanding of the LC biomechanics and guide its future mathematical and numerical modeling.

2 Mathematical Modeling

Mathematical modeling is an attractive tool in understanding the behavior of structures. With the closed form solutions obtained, the influence of various parameters and modeling idealizations can be directly recognized and parametric studies easily performed. However, as mathematical modeling is only practically feasible for simple structures, idealizations are often necessary and analysts need to select the parameters expected to have the greatest influence for inclusion in the model. Undoubtedly, more complex analysis can be conducted using other approaches such as the finite element or finite difference method. However, closed form mathematical modeling should be seen as an important first step to provide an insight into the importance of parameters, to create useful benchmarks for future calibration exercises and to develop simple, approximate “engineering” methods for initial analysis and interpretation.

In modeling the LC, there is uncertainty regarding a number of aspects, mainly:

- the boundary condition, i.e., whether the LC is only simply supported along the interface with the sclera or is there additional restraint against rotation along this line
- the effect of in-plane pretension due to scleral expansion
- the relative importance of the in-plane and flexural stiffness of the LC
- the spatial heterogeneity in the biomechanical properties of the LC
- the constitutive relationship of the lamina cribrosa material

This study is intended to help clarify the current uncertainty and guide decisions on how to include these factors in future modeling

work. Only the first three factors are included at this stage. The fourth and fifth factors, which require both experimental and mathematical studies, are the focus of the next stage of research. However, in the absence of specific experimental data the constitutive relationship reported by Woo et al. [11] will be used to represent the material behavior.

The work presented benefits from the efforts made earlier to produce general solutions for circular plates with various loading and boundary conditions. The most notable contributions were made by Timoshenko and Woinowsky-Krieger [12]. The following six mathematical models are built on different modeling idealizations, which are devised to enable assessing the importance of the first three factors. A brief description of these idealizations is provided in Table 1 and free body diagrams for each of the models are shown in Fig. 2.

2.1 Model 1 With a Clamped Edge and No In-Plane Pretension. The first model ignores in-plane pretension due to scleral expansion and assumes the sclera provides the LC with a clamped edge, where rotation but not in-plane deformation is prevented. This recognizes that the 0.12 mm thick LC is much thinner than the surrounding 1.0 mm thick sclera. This model assumes the LC to be homogeneous, isotropic and with a uniform thickness. It also assumes that out-of-plane deformation is small compared with the LC dimensions, and as a result, the changes in the thickness of the plate with deformation are ignored. From analysis of a plate segment bounded by two diametral and two cylindrical sections (Fig. 3) and considering the following boundary conditions:

- the deflection along the plate edge is prevented and
- the slope of the deflection surface along the edge and at the center is zero

The retrodisplacement of the uniformly loaded LC, w , at any

Table 1 Modeling idealization considered in models 1–6

Model	Edge with sclera	In-plane pre-tension due to scleral expansion	Other features
1	Clamped	Ignored	Small deflection model
2	Simple	Ignored	Small deflection model
3	Clamped	Considered	Small deflection model
4	Simple	Considered	Small deflection model
5	Clamped	Ignored	Large deflection model
6	Simple	Ignored	Membrane model

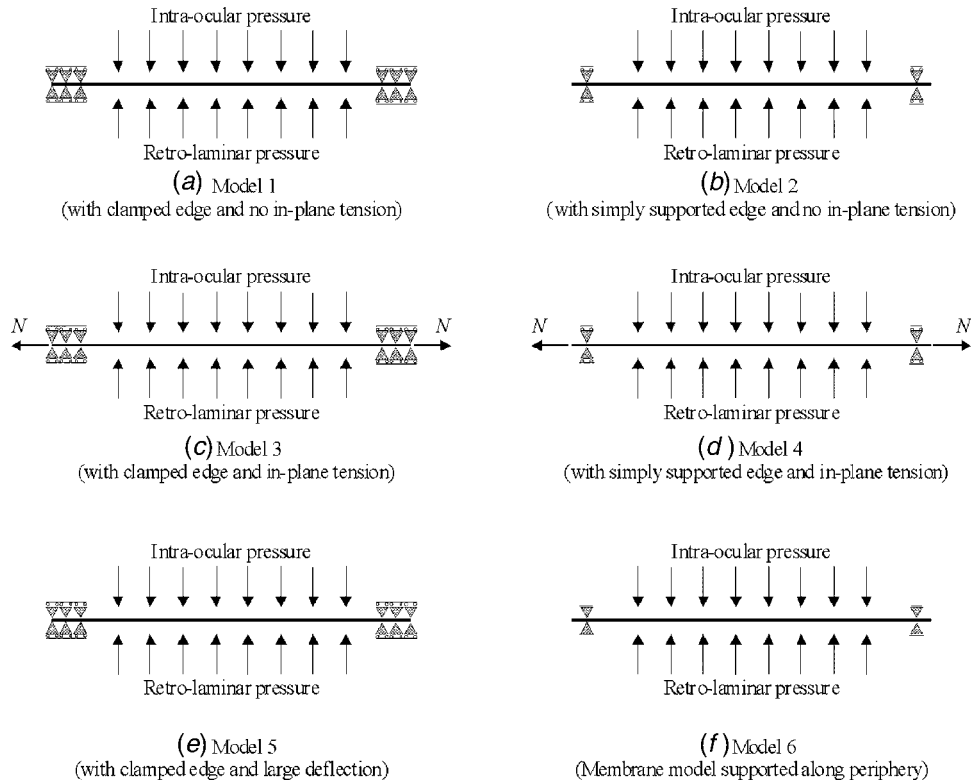


Fig. 2 Free body diagrams of the modeling idealizations in models 1–6

point at distance r from the center is given by Timoshenko and Woinowsky-Krieger [12] using the circular plate theory as

$$w = \frac{q(R^2 - r^2)^2}{64D} \quad (1)$$

where R is the radius of the LC, D is the flexural rigidity of the LC, $D = Eh^3/12(1-\nu^2)$, E is the elastic (Young's) modulus, h is the LC thickness, ν is Poisson's ratio, $q = \text{IOP} - S$, the difference between the IOP and the retrolaminar pressure (S —also called the optic nerve tissue pressure). S is given as a function of IOP [8,3] in the form

$$S = 0.5\text{IOP} \quad \text{for IOP} < 20 \text{ mm Hg} \quad \text{and} \\ S = 10 \text{ mm Hg} \quad \text{for IOP} > 20 \text{ mm Hg}$$

From the following equations relating the radial and tangential bending stresses, σ_r and σ_t , to the displacement, w :

$$\sigma_r = \frac{6D}{h^2} \left(\frac{d^2w}{dr^2} + \frac{\nu}{r} \frac{dw}{dr} \right) \quad \text{and} \quad \sigma_t = \frac{6D}{h^2} \left(\frac{1}{r} \frac{dw}{dr} + \nu \frac{d^2w}{dr^2} \right) \quad (2)$$

the stresses can be obtained as

$$\sigma_r = -\frac{3q}{8h^2} [R^2(1+\nu) - r^2(3+\nu)] \quad \text{and}$$

$$\sigma_t = -\frac{3q}{8h^2} [R^2(1+\nu) - r^2(1+3\nu)] \quad (3)$$

At the center ($r=0$), the retrodisplacement and the stresses become

$$w_{r=0} = \frac{qR^4}{64D}, \quad (\sigma_r)_{r=0} = (\sigma_t)_{r=0} = -\frac{3qR^2(1+\nu)}{8h^2} \quad (4)$$

and at the edge of the plate (where $r=R$)

$$w_{r=R} = 0, \quad (\sigma_r)_{r=R} = \frac{3qR^2}{4h^2} \quad \text{and} \quad (\sigma_t)_{r=R} = \frac{3\nu qR^2}{4h^2} \quad (5)$$

Note that

- While w is highest at the center, σ_r is highest along the plate edge.
- At the plate center, the stresses calculated using Eq. (4) cause tension on the posterior side and compression on the anterior side. The opposite is true along the edge where Eq. (5) is used.

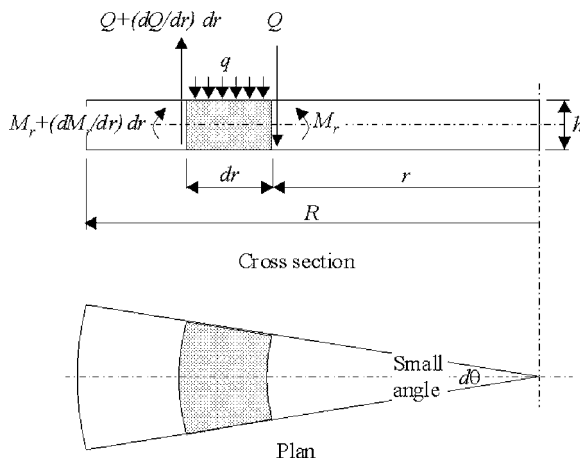


Fig. 3 Analysis of a laterally loaded circular plate (see Ref. [12])

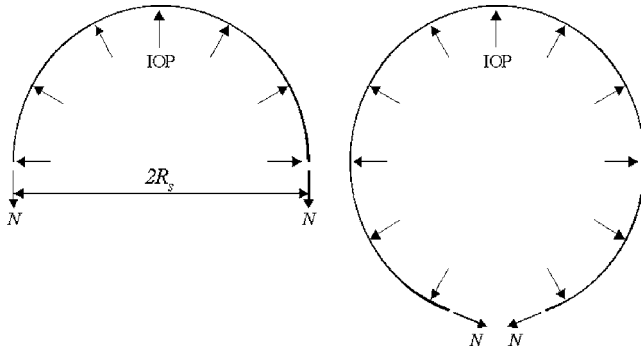


Fig. 4 Equilibrium of the sclera

2.2 Model 2 With a Simply Supported Edge and No In-Plane Pretension. Another idealization of the LC is based on reducing the importance of the rotational restraint provided by the sclera. The model in this case is obtained from model 1 by releasing the restraint against edge rotation and therefore applying an edge bending moment equal and opposite to that developed by the edge clamp of model 1.

In model 1, the bending moment along the edge clamp is

$$M_r = -\frac{\sigma_{r(r=R)}h^2}{6} = -\frac{qR^2}{8} \quad (6)$$

Applying an equal and opposite moment of magnitude $qR^2/8$ along the plate edge while allowing it to rotate there results in the following distribution of deflection:

$$w = \frac{qR^2}{16D(1+\nu)}(R^2 - r^2) \quad (7)$$

Adding this to the deflection of the clamped plate in Eq. (1), results in the deflection of a simply supported plate

$$w = \frac{q(R^2 - r^2)}{64D} \left(\frac{5+\nu}{1+\nu} R^2 - r^2 \right) \quad (8)$$

The stresses σ_r and σ_t , are also obtained in the same manner as

$$\sigma_r = -\frac{3q}{8h^2}(3+\nu)(R^2 - r^2) \quad \text{and} \quad \sigma_t = -\frac{3q}{8h^2}[R^2(3+\nu) - r^2(1+3\nu)] \quad (9)$$

w and σ_r given in Eqs. (8) and (9) have zero values along the edge and a parabolic distribution inside the plate. The maximum values for the retrodisplacement, w , and the stresses, σ_r and σ_t , exist at the center, where $r=0$:

$$w_{\max} = \frac{qR^4(5+\nu)}{64(1+\nu)D} \quad \text{and} \quad (\sigma_r)_{\max} = (\sigma_t)_{\max} = -\frac{3qR^2(3+\nu)}{8h^2} \quad (10)$$

Note that the stresses calculated using Eq. (10) are tensile on the posterior side of the LC and compressive on the anterior side.

2.3 Model 3 With a Clamped Edge and In-Plane Pretension. The in-plane pretension in this model arises from the scleral expansion due to the application of the IOP. The value of the pretension, N , can be derived by analyzing the sclera as an idealized perfect sphere. Equilibrium of the scleral hemisphere under IOP and N leads to (Fig. 4)

$$N(2\pi R_s) = \text{IOP}\pi R_s^2 \quad \text{or} \quad N = \frac{\text{IOP}R_s}{2} \quad (11)$$

where R_s is the radius of the sclera.

The effect of in-plane pretension on the retrodisplacement of a circular plate has been obtained earlier by Dongqi and Zeqin [8] in the form

$$w = \frac{w_q}{1+\alpha} \quad (12)$$

where w_q is the retrodisplacement for an equivalent plate without in-plane forces (as given in Eq. (1)), and $\alpha = NR^2/14.68D$. Substituting the values of N and α in Eq. (12), w is obtained as

$$w = \frac{29.36Dw_q}{29.36D + \text{IOP}R_s R^2} = Aw_q, \quad (13)$$

where $A = 29.36D/29.36D + \text{IOP}R_s R^2$. The stresses, σ_r and σ_t , can then be obtained using the equations

$$\sigma_r = \sigma_{r1} + \sigma_{r2}, \quad \text{where} \quad \sigma_{r1} = -\frac{3Aq}{8h^2}[R^2(1+\nu) - r^2(3+\nu)], \quad \sigma_{r2} = \frac{N}{h}, \quad \text{and} \quad (14)$$

$$\sigma_t = \sigma_{t1} + \sigma_{t2}, \quad \text{where} \quad \sigma_{t1} = -\frac{3Aq}{8h^2}[R^2(1+\nu) - r^2(1+3\nu)], \quad \sigma_{t2} = \frac{N}{h} \quad (15)$$

In Eqs. (14) and (15) σ_{r1} and σ_{t1} are caused by the lateral load q , while σ_{r2} and σ_{t2} are due to the in-plane pretension. Note that while σ_{r1} and σ_{t1} are tensile on the posterior side of the plate and compressive on the anterior side, σ_{r2} and σ_{t2} are always tensile.

2.4 Model 4 With a Simply Supported Edge and In-Plane Pretension. The development of this model is similar to model 3. The retrodisplacement of the LC again takes the form in Eq. (12), but w_q in this case is obtained from Eq. (8) from model 2 with a simply supported edge. In this case, α is also different according to Timoshenko and Woinowsky-Krieger [12]

$$\alpha = \frac{NR^2}{4.20D} \quad (16)$$

As a result, the deflection w is obtained as

$$w = \frac{8.4Dw_q}{8.4D + \text{IOP}R_s R^2} = Bw_q \quad (17)$$

where

$$B = \frac{8.4D}{8.4D + \text{IOP}R_s R^2} \quad (18)$$

The stresses are obtained in a similar fashion to model 3 in the form

$$\sigma_r = \sigma_{r1} + \sigma_{r2} \quad \text{and} \quad \sigma_t = \sigma_{t1} + \sigma_{t2} \quad (19)$$

where

$$\sigma_{r1} = -\frac{3Bq}{8h^2}(3+\nu)(R^2 - r^2) \quad (20)$$

$$\sigma_{t1} = -\frac{3Bq}{8h^2}[R^2(3+\nu) - r^2(1+3\nu)] \quad \text{and} \quad (21)$$

$$\sigma_{r2} = \sigma_{t2} = \frac{N}{h} = \frac{\text{IOP}R_s}{2h} \quad (22)$$

2.5 Model 5 With a Clamped Edge and Large Deflection. In the above four models, the deflections are assumed to be

smaller than the plate thickness. As a result, the strain at the middle plane of the plate is assumed to be small and negligible. However, if the deflection is no longer assumed to be smaller than the thickness, yet still small in comparison with other dimensions, the strain of the middle plane must be considered. An approximate solution for this problem is provided by Timoshenko and Woinowsky-Krieger [12] in the form

$$w = \frac{\eta q (R^2 - r^2)^2}{64D}, \quad (23)$$

$$\sigma_r = -\frac{3\eta q}{8h^2} [R^2(1+\nu) - r^2(3+\nu)] \quad \text{and}$$

$$\sigma_t = -\frac{3\eta q}{8h^2} [R^2(1+\nu) - r^2(1+3\nu)] \quad (24)$$

where $\eta = 1/1 + 0.488(w_0^2/h^2)$, defines the effect of the stretching of the middle plane on the plate deflection, and w_0 is the retrodisplacement at the center. Note that while large deflections are considered in the development of Eqs. (23) and (24), the corresponding thickness change under load is ignored for simplicity. In solving Eqs. (23) and (24), Eq. (23) is rewritten for the center point ($r=0$) as

$$w_0 = \frac{qR^4}{64D} \frac{1}{1 + 0.488 \frac{w_0^2}{h^2}} \quad (25)$$

This third order equation is first solved for w_0 . Then the distribution of w can be obtained from $w = w_0(1 - r^2/R^2)^2$ and σ_r and σ_t from Eq. (24). Notice that the parameter η increases in significance with large deformation. For instance, for $w_0 = 0.5h$, η equals 0.89. With w_0 increasing to $h, 2h$, and $4h$, η becomes 0.67, 0.34, and 0.11 respectively. This means that the plate stiffness grows gradually with larger deformation.

2.6 Model 6 With the LC Modeled as a Membrane Supported Along Its Periphery. As a step further from the above model, model 6 assumes the plate has no flexural stiffness and its behavior under lateral pressure is dominated by the membrane action. The model again assumes that w has the same dependence on r as in other models

$$w = w_0 \left(1 - \frac{r^2}{R^2}\right)^2 \quad (26)$$

The derivation of w_0 for a circular membrane follows a strain-energy/virtual deflection approach, which is common in stress-strain problems of this kind. The radial and transverse strains, ε_r and ε_t , and the radial displacement, u , at radius r are given by

$$\varepsilon_r = \frac{du}{dr} + \frac{1}{2} \left(\frac{dw}{dr}\right)^2 \quad (27)$$

$$\varepsilon_t = \frac{u}{r} \quad (28)$$

$$u = r(R - r)(c_1 + c_2r) \quad (29)$$

where c_1 and c_2 are constants. The strain energy in the LC associated with the stretching of the membrane is given by

$$V = \frac{\pi E h}{1 - \nu^2} \int_0^R (\varepsilon_r^2 + \varepsilon_t^2 + 2\nu\varepsilon_r\varepsilon_t) r dr \quad (30)$$

To calculate the deflection of the membrane, the above equations are solved to find c_1 , c_2 , and w_0 . First, the right sides of Eqs. (26)–(29) are substituted for the corresponding terms in Eq. (30). Using the resulting form of Eq. (30), c_1 and c_2 are found by imposing the requirements that

Table 2 Material properties for the lamina cribrosa as given by Woo et al. (see Ref. [11]). Note: MPa=N/mm² and kPa =0.001 N/mm².

	G (MPa)	E(MPa)	Range of stress (kPa)	
			From	To
Lamina cribrosa	0.12	0.358	0.0	8.0
	0.22	0.656	8.0	15.0
	0.61	1.818	15.0	–

$$\frac{\partial V}{\partial c_1} = 0 \quad \text{and} \quad \frac{\partial V}{\partial c_2} = 0$$

Another requirement is introduced that the change in the work done by the differential pressure acting through a virtual displacement equals the change in strain energy associated with the virtual displacement. If the virtual displacement is chosen as δw (which is directly proportional to w_0), this requirement can be expressed by the equation

$$\frac{\partial V}{\partial w_0} \delta w_0 = 2\pi q \delta w_0 \int_0^R \left[1 - \left(\frac{r}{R}\right)^2\right]^2 r dr \quad (31)$$

After manipulation and following the procedure presented in Ref. [13], the solution for the maximum displacement can finally be presented as

$$w_0 = \beta R \sqrt[3]{\frac{qR}{Eh}} \quad (32)$$

where

$$\beta = \sqrt[3]{\frac{6615(\nu^2 - 1)}{2(2791\nu^2 - 4250\nu - 7505)}}$$

and therefore w is determined as

$$w = \sqrt[3]{\frac{6615(\nu^2 - 1)}{2(2791\nu^2 - 4250\nu - 7505)}} R \sqrt[3]{\frac{qR}{Eh}} \left(1 - \frac{r}{R}\right)^2 \quad (33)$$

By using $\nu=0.49$ (according to Woo et al. [11]), we obtain $w_0 = 0.65R \sqrt[3]{qR/Eh}$. The membrane stress, σ_r , (i.e., the in-plane radial stress due to the membrane action) is also obtained as

$$(\sigma_r)_{r=0} = 0.414 \sqrt[3]{\frac{Eq^2R}{h^2}} \quad \text{and} \quad (\sigma_r)_{r=R} = 0.321 \sqrt[3]{\frac{Eq^2R}{h^2}}. \quad (34)$$

3 Comparative Study of Mathematical Models

A brief comparative study of the six mathematical models developed above is conducted to identify the effect of various idealizations. All six models are used to predict the central displacement of the LC under a range of IOP between 10 and 60 mm Hg (0.00133, and 0.0079 N/mm²), or q (= IOP—the retro-laminar pressure) between 5 and 50 mm Hg (0.00067, and 0.006,67 N/mm²). The LC and scleral dimensions used are as reported by Yan et al. [14], Woo et al. [11], and Dongqi and Zeqin [8]: R = LC radius =0.6 mm, h =LC thickness =0.12 mm, R_s = scleral radius =12 mm, and h_s = scleral thickness =1 mm.

The shear modulus, G , of the LC is assumed to be that given by Woo et al. [11] in the form of the trilinear relationships shown in Table 2. The modulus of elasticity, E , is derived from the shear modulus using the relation $G=E/2(1+\nu)$, where ν is Poisson's ratio, taken as 0.49. For each IOP increment, calculations are made for q (=IOP- S), stresses (σ_r and σ_t), E (Table 2), D ($Eh^3/12[1-\nu^2]$) and w . Due to the trilinear expression used for E , the relationship between pressure and deformation is nonlinear.

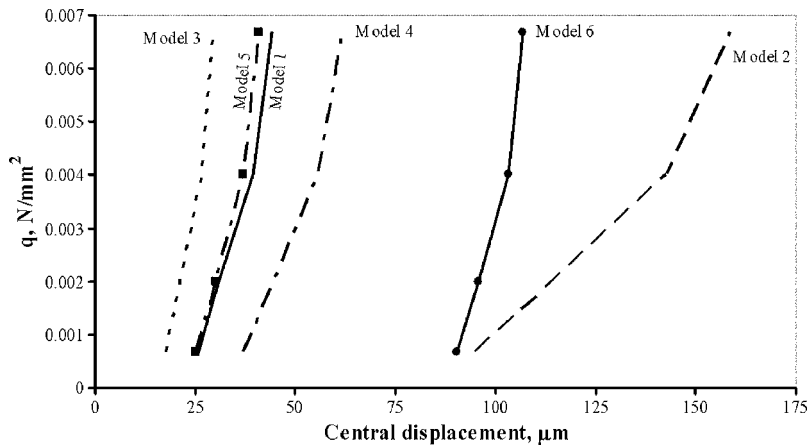


Fig. 5 Central displacement comparisons between the mathematical models

The central displacements obtained from the six models are compared in Fig. 5. The following observations can be made:

- The edge fixity has a large effect on the model predictions. Models 2 and 4 with simply supported edges deform considerably more than models 1 and 3 with clamped edges (by 268% and 110%, respectively).
- Introducing the in-plane pretension caused by scleral expansion also has a notable effect. It reduces the displacement of the model with a simply supported edge (model 2) by 61% and the model with a clamped edge (model 1) by 32%.
- Modifying the mathematical model to recognize large deformations (model 5) leads to relatively small effects on the results (below 5%). This is due to the fact that the deformations obtained under the largest IOP considered did not exceed 35% of the thickness of the lamina cribrosa.
- Modeling the LC as a membrane results in large displacement predictions, but the stiffness of the membrane increases rapidly with more curvature as would be expected.

Reference can also be made to Fig. 6 showing the distribution of model displacement across the LC diameter under IOP = 25 mm Hg (i.e., $q = 15$ mm Hg or 0.002 N/mm², allowing for a retrolamina pressure $S = 10$ mm Hg). The observations noted above regarding the central displacement predictions are also valid when comparing the displacement distributions in this figure. Notice also the reduced displacement near the model edge in cases with clamped boundary conditions.

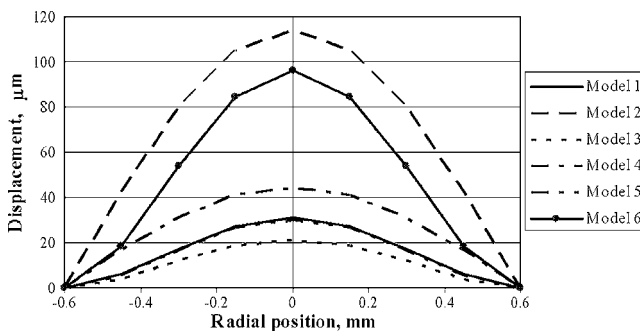


Fig. 6 Distribution of displacement across LC diameter under IOP=25 mm Hg ($q = 15$ mm Hg or 0.002 N/mm²) as predicted by mathematical models

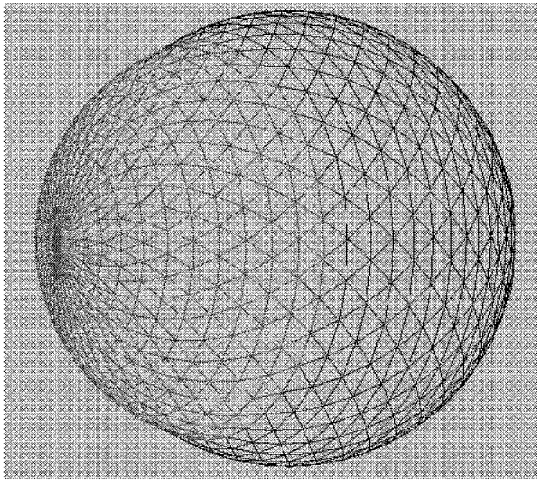
4 Further Assessment of Models

In this section, the predictions of the six models are also compared against the results of a nonlinear finite element (FE) model of the whole eye. This numerical model, which incorporates the lamina cribrosa, the sclera, and the cornea, is not based on any a priori assumptions of the LC's boundary conditions, e.g., in-plane pretension, etc. The FE model has been constructed in this form to provide comparative predictions and to guide the selection of the most suitable closed-form mathematical model for predicting the behavior of the LC. This model has been used successfully to predict the biomechanical performance of the cornea under elevated IOP in an earlier study [15]. In this work it is intended to make up for the current paucity of available experimental data in validating the mathematical models presented herein. However, it should be the aim of future work to address this shortfall and make available reliable laboratory data on the LC behavior.

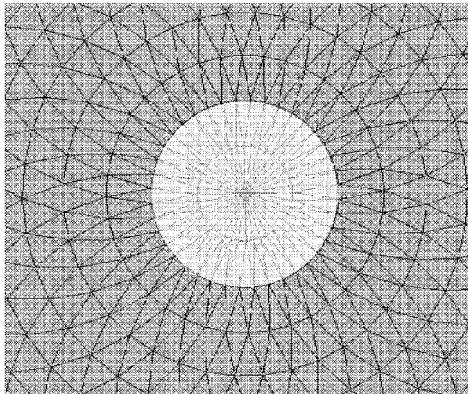
The nonlinear FE model uses 4000 linear strain, triangular elements arranged in 40 layers, with 100 elements per layer (see Figs. 7(a) and 7(b)). General purpose thin shell elements are used throughout for their ability to cope with small as well as large deformations. Each element has three corner nodes with six degrees of freedom per node ($u, v, w, \theta_x, \theta_y, \theta_z$). The model is built using Abaqus FE software package [16]. The analyses consider both geometric nonlinearities due to change of joint coordinates and material nonlinearities according to the relationships given in Tables 2 and 3. In tracing the nonlinear behavior, Riks arc method is adopted [17]. In this method, load increments vary according to the current stage of overall behavior, and are controlled automatically such that a solution is obtained even close to the points of instability. The model is supported at three points along the main circle of the sclera, which is parallel to the corneo-scleral intersection. This choice of boundary conditions was adopted so that it has the minimum effect on the behavior of the LC part of the model.

The construction of the FE model is based on an earlier study to optimize the finite element analysis of the eye globe [15]. The study considered several aspects including the density of the finite element mesh, the thickness variation within the cornea, and the significance of the out-of-plane flexural and torsional resistance of the globe components. The study confirmed the importance of using a dense mesh and incorporating the out-of-plane resistance components. Modeling the thickness variation of the cornea did not lead to notable variation in overall behavior predictions. While detailed validation and calibration of the whole eye globe finite element model (including the geometric and constitutive assumptions) is still in progress, this approach has provided a benchmark for assessing the mathematical models presented in this paper.

The dimensions used in the model are: lamina cribrosa:



(a) Finite element mesh of full eye globe, seen from corneal side



(b) Mesh around the lamina cribrosa, at rear of eye (LC shown in light shading)

Fig. 7 Details of the finite element meshes used in analysis

$R=R_{LC}=0.6$ mm, $h=LC$ thickness=0.12 mm; cornea: $R_c=R_{cornea}=6$ mm, $h_c=h_{cornea}=0.6$ mm; and sclera: $R_s=R_{sclera}=12$ mm and $h_s=h_{sclera}=1.0$ mm.

The moduli of elasticity of the cornea and the sclera are derived from the trilinear relationships given by Woo et al. [11] for the shear modulus, G , and assuming $\nu=0.49$. The results are listed in Table 3.

Table 3 Material properties for the cornea and the sclera as given by Woo et al. (see Ref. [11]). Note: MPa=N/mm² and kPa=0.001 N/mm².

	G (MPa)	E (MPa)	Range of stress (kPa)	
			From	To
Cornea	0.18	0.536	0.0	4.0
	0.37	1.103	4.0	12.5
	0.81	2.414	12.5	–
	0.90	2.682	0.0	10.0
Sclera	1.40	4.172	10.0	22.0
	2.70	8.046	22.0	–

The model was subjected to an IOP range between 10 and 60 mm Hg (0.0013 and 0.0079 N/mm²). IOP was applied as a uniform pressure acting on the internal faces of all elements forming the model. The LC was additionally subjected to the corresponding retrolaminar pressure in accordance with the relations given in model 1. The central displacement of the LC part of the model, relative to the surrounding sclera, was compared to the predictions of the six mathematical models and the results are given in Fig. 8. The comparisons show clearly that model 3 with a clamped edge and in-plane pretension achieved the closest agreement with the FE model. Adopting simple edge supports or modeling the lamina cribrosa as a membrane clearly resulted in an overestimated displacement compared with the FE model. The error margin associated with model 3 was below 10% at all IOP levels. Ignoring the in-plane pretension caused by scleral expansion (as in model 1) caused a growth in the error margin to between 35% and 45%. Enabling the model to consider large out-of-plane deflections reduced the errors slightly and made it evident that the in-plane pretension was a more influential factor than the accurate modeling of the large deflections.

The distribution of displacement across the LC diameter under IOP =25 mm Hg is also plotted in Fig. 9 as obtained by the FE and the six mathematical models. The close correlation with model 3 is maintained across the whole diameter. There is also strong evidence of very limited rotation along the LC edge in the FE model, indicating a behavior pattern close to that associated with a clamped edge.

These findings show the importance of in-plane pretension and the edge fixity provided by the sclera in modeling the behavior of the LC. Future work, whether closed-form mathematical or numerical, could build on these findings in the efforts to study the

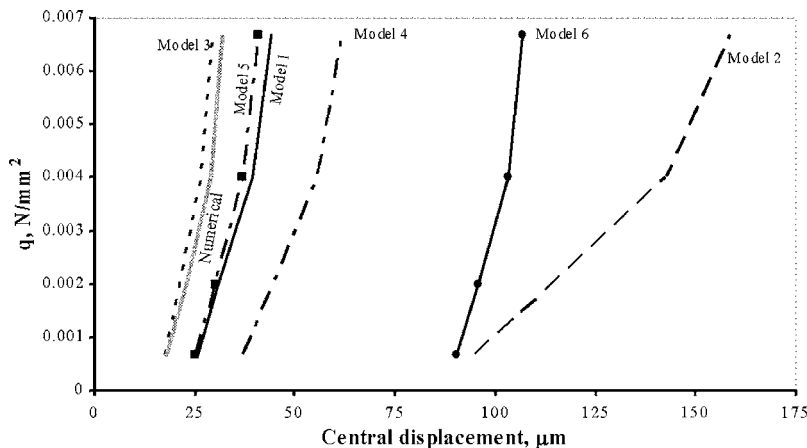


Fig. 8 Central displacement comparisons between the FE and mathematical models

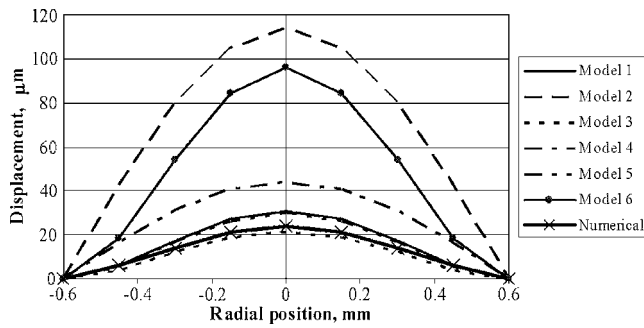
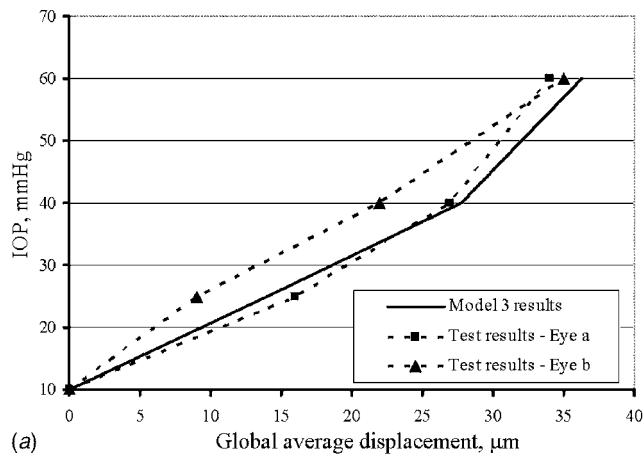


Fig. 9 Distribution of displacement across the LC diameter under IOP =25 mm Hg according to the finite element and the mathematical models

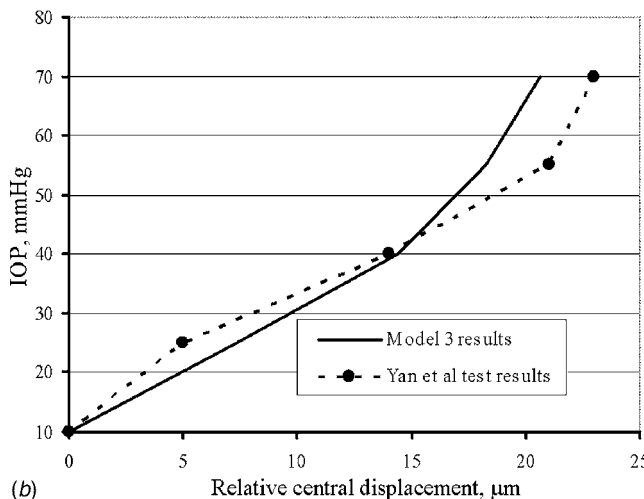
mechanics of the LC and also the importance of other factors, such as viscoelasticity and the structural support of the axons.

5 Assessment Against Experimental Data

A further assessment of the most successful model (compared to the finite element analysis), number 3, is done by comparing its predictions to results of experimental testing reported by Levy and Crapps [5] and by Yan et al. [18] on LC specimens. The dimensions used in the mathematical modeling are: $R=0.6$ mm, $h=0.120$ mm, $R_s=12.0$ mm, and $h_s=1.0$ mm.

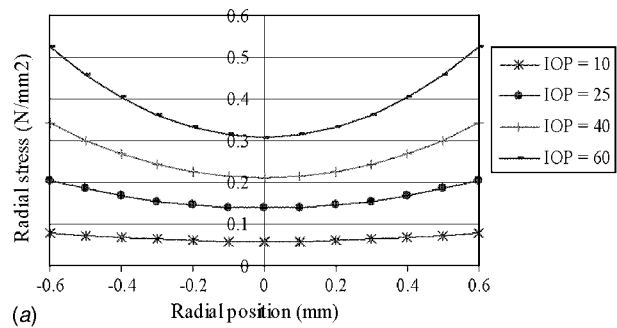


(a)

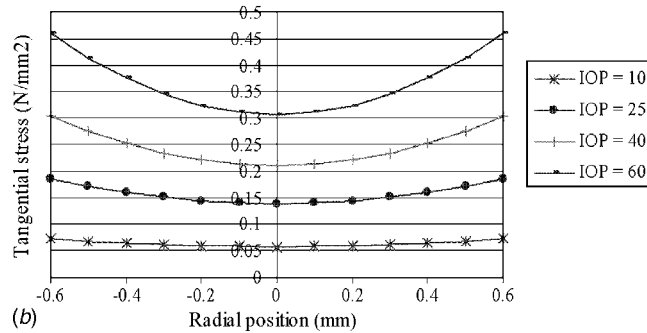


(b)

Fig. 10 Comparison between model 3 predictions and earlier experimental data



(a)



(b)

Fig. 11 Stress distribution on the anterior face of the lamina cribrosa at four different levels of IOP as obtained using model 3

The resulting model predictions match closely the test data as shown in Fig. 10. The comparisons start at IOP=10 mm Hg as this pressure was needed in the experiments to ensure the specimens had been inflated and become free of wrinkles. Hence, the displacements are relative to this geometric datum and have been corrected for the appropriate retrolamina pressure. Note also that the comparisons with the Levy and Crapps [5] results refer to the global average displacements of the LC. In these tests, the profile of the LC was monitored under elevated IOP and the average displacement (rather than the central displacement) was reported in their paper.

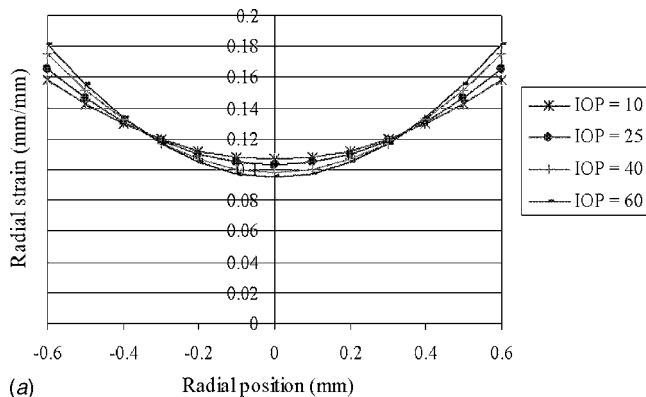
6 Stress And Strain Distribution

The distributions of stress and strain across the diameter of the lamina cribrosa, as obtained using model 3, are illustrated in Figs. 11 and 12, respectively. The dimensions and material properties used are: $h=0.12$ mm, $R=0.6$ mm, $R_s=12$ mm, and $\nu=0.49$. The modulus of elasticity, E_{LC} , is taken as 0.358 MPa as given in Table 2.

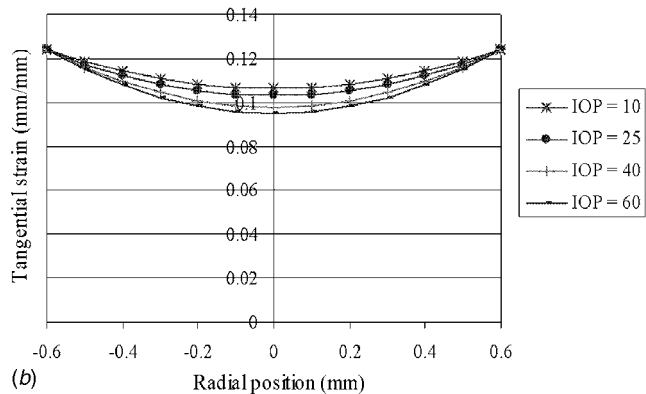
The stresses and strains are significantly higher along the edges of the lamina cribrosa and gradually reduce towards the center. This observation ties closely with the earlier finding by Garway-Heath et al. [19] that the loss of vision in glaucomatous eyes starts along the boundaries and grows towards the center. The retinal axons responsible for transmitting the vision signals along the boundaries are known to cross the lamina cribrosa near its edge. It appears therefore that the high stresses and strains in the LC edge could be responsible for damage to the axons transmitting the boundary vision signals. Then with higher IOP, the stresses and strains closer to the center of the LC grow, spreading the damage to the axons transmitting vision signals from more central areas.

7 Conclusions

Six mathematical approaches to the biomechanical modeling of the LC are introduced in this paper. In particular, the LC boundary condition, the effect of the surrounding sclera, and the relative significance of in-plane and flexural stiffness are varied between the models. Comparisons with a full ocular finite element model,



(a)



(b)

Fig. 12 Strain distribution on the anterior face of the lamina cribrosa at four different levels of IOP as obtained using model 3

which does not adopt any related idealizations, indicate that considering a clamped edge and incorporating in-plane pretension are important modeling considerations. With these factors included in the closed-form mathematical model based on the circular plate theory, predictions of the behavior of the LC under elevated IOP have been achieved with good agreement with FE model and with limited available experimental data. Further, the following conclusions are drawn from the research presented in this paper:

1. The effects of boundary conditions (i.e., end fixity) and in-plane pretension on the outcome of mathematical modeling are significant. Therefore, care should be taken in considering these factors when attempting to approximate in vivo conditions.
2. Modeling the lamina cribrosa as a membrane leads to large overestimations of the displacement compared with the results of FE modeling and the limited available experimental data.
3. With a relatively simple closed-form mathematical model that incorporates the most pertinent aspects, the behavior of the lamina cribrosa could be reasonably accurately predicted, enabling parametric studies to be conducted

easily using calculations that could be developed rapidly by hand or using a spreadsheet.

4. Further model development should be conducted to ascertain whether a more accurate representation of the structural complexity of the lamina cribrosa would produce improved predictions of the biomechanical behavior under elevated intraocular pressure.

Acknowledgment

This work was partially supported by an award from the Royal Society of London, UK. The authors are grateful for the valuable contributions made by David Garway-Heath, the lead clinical researcher of the Glaucoma Research Unit, Moorfields Hospital, London.

References

- [1] Anderson, D. R., 1995, "Glaucoma, Its Terminology and Fundamental Nature," *Optic Nerve in Glaucoma*, S. M. Dance, ed., Kugler, New York, pp. 1–14.
- [2] Emery, J. M., Landis, D., Paton, D., Boniuk, M., and Craig, J. M., 1974, "The Lamina Cribrosa in Normal and Glaucomatous Human Eyes," *Trans. Am. Acad. Ophthalmol. Otolaryngol.*, **78**, pp. OP290–OP297.
- [3] Quigley, H. A., 1986, "Pathophysiology of Optic Nerve in Glaucoma," *Glaucoma*, J. A. McAllister and R. P. Wilson, eds. Butterworths, London, pp. 30–53.
- [4] Harju, M., 2001, "Exfoliation Glaucoma: Studies on Intraocular Pressure, Optic Nerve Head Morphometry, and Ocular Blood Flow," Academic Dissertation, Department of Ophthalmology, Haartmaninkatu, Helsinki, Section: Theories of Glaucoma.
- [5] Levy, N. S., and Crapps, E. E., 1984, "Displacement of Optic Nerve Head in Response to Short-Term Intraocular Pressure Elevation in Human Eyes," *Arch. Ophthalmol. (Chicago)*, **102**(5), pp. 782–786.
- [6] Quigley, H. A., Hohman, R. M., Addicks, E. M., Massof, R. W., and Green, W. R., 1983, "Morphologic Changes in the Lamina Cribrosa Correlated With Neural Loss in Open-Angle Glaucoma," *Am. J. Ophthalmol.*, **95**(5), pp. 673–91.
- [7] Chi, T., Ritch, R., and Stickler, D., 1989, "Racial Differences in Optic Nerve Head Parameters," *Arch. Ophthalmol. (Chicago)*, **107**, pp. 836–839.
- [8] Dongqi, H., and Zeqin, R., 1999, "A Biomathematical Model for Pressure-Dependent Lamina Cribrosa Behavior," *J. Biomech.*, **32**(6), pp. 579–84.
- [9] Edwards, M. E., and Good, T. A., 2001, "Use of a Mathematical Model to Estimate Stress and Strain During Elevated Pressure Induced LC Deformation," *Curr. Eye Res.*, **23**(3), pp. 215–25.
- [10] Bellezza, A. J., Hart, R. T., and Burgoyne, C. F., 2002, "The Optic Nerve Head as a Biomechanical Structure," *Invest. Ophthalmol. Visual Sci.*, **41**(10), pp. 2991–3000.
- [11] Woo, S. L., Kobayashi, A. S., Schlegel, W. A., and Lawrence, C., 1972, "Non-linear Material Properties of Intact Cornea and Sclera," *Exp. Eye Res.*, **14**(1), pp. 29–39.
- [12] Timoshenko, S. P., and Woinowsky-Krieger, S., 1970, *Theory of Plates and Shells*, McGraw-Hill, New York.
- [13] NASA, 1998, "Deflection of Circular Membrane Under Differential Pressure," Report No. GSC-13783, NASA Tech Briefs, 22(5), p. 78; available online: <http://www.nasatech.com/Briefs/May98/GSC13783.html>.
- [14] Yan, D. B., Coloma, F. M., Metheerairut, A., Trope, G. E., Heathcote, J. G., and Ethier, C. R., 1994, "Deformation of the Lamina Cribrosa by Elevated Intraocular Pressure," *Br. J. Ophthalmol.*, **78**(8), pp. 643–648.
- [15] Anderson, K., El-Sheikh, A., and Newson, T., 2004, "Application of Structural Analysis to the Mechanical Behaviour of the Cornea," *Interface (USA)*, **1**, pp. 1–13.
- [16] Hibbitt, Karlsson, and Sorensen, Inc., 2004. Abaqus—Standard Users Manual, Detroit.
- [17] Riks, E., 1972, "The Application of Newton's Method to the Problem of Elastic Stability," *ASME J. Appl. Mech.*, **39**, pp. 1060–1066.
- [18] Yan, D. B., Flanagan, J. G., Farra, T., Trope, G. E., and Ethier, C. R., 1998, "Study of Regional Deformation of the Optic Nerve Head Using Scanning Laser Tomography," *Curr. Eye Res.*, **17**(9), pp. 903–916.
- [19] Garway-Heath, D. F., Poinoosawmy, D., Fitzke, F. W., and Hitchings, R. A., 2000, "Mapping the Visual Field to the Optic Disc in Normal Tension Glaucoma Eyes," *Ophthalmology*, **107**, pp. 1809–1815.